





## Direct observations of causal links in plastic events and relevance to earthquake seismology

Pinaki Kumar <sup>1,2</sup> Roberto Benzi <sup>3</sup> Jeannot Trampert <sup>4</sup> and Federico Toschi <sup>1,2</sup>

<sup>1</sup>*Department of Applied Physics and Science Education, Eindhoven University of Technology, P.O. Box 513, 5600 MB Eindhoven, The Netherlands*

<sup>2</sup>*CNR-IAC, 00185 Rome, Italy*

<sup>3</sup>*Department of Physics, University of “Tor Vergata”, Via della Ricerca Scientifica 1, 00133 Rome, Italy*

<sup>4</sup>*Department of Earth Sciences, Utrecht University, Princetonlaan 8a, 3594 CB Utrecht, The Netherlands*



(Received 8 December 2022; accepted 7 September 2023; published 25 September 2023)

Earthquakes are complex physical processes driven by stick-slip motion on a sliding fault. After the main event, a series of aftershocks is usually observed. The latter are loosely defined as earthquakes that follow a parent event and occur within a prescribed space-time window. In seismology, it is currently not possible to establish an unambiguous causal relation between events, and the nearest-neighbor metric is commonly used to distinguish aftershocks from independent events. Here, we employ a soft-glass model as a proxy for earthquake dynamics, previously shown to be able to correctly reproduce the phenomenology of earthquakes, together with a technique that allows us to clearly separate independent and triggered events. We show that aftershocks in our plastic event catalog follow Omori’s law with slopes depending on the triggering mode, an observation possibly useful for seismology. Finally, we confirm that the nearest-neighbor metric is indeed effective in separating independent events from aftershocks.

DOI: [10.1103/PhysRevResearch.5.033211](https://doi.org/10.1103/PhysRevResearch.5.033211)

### I. INTRODUCTION

Aftershocks are earthquakes that follow a given event and occur within prescribed space-time windows. The notion of aftershocks, therefore, implies causality. Separate fields of science dealing with dynamical systems treat causality very differently, varying from a theoretical notion in physics [1] to a common-sense approach in the legal domain [2], via a complex system analysis in epidemiology [3] to name just a few. Establishing causality between events can take the form of direct perception, logical reasoning, or statistical tests of varying sophistication. In certain cases, after the careful exclusion of confounding variables, one observes that when a certain action/event occurs, another event always occurs later in time, and when the former event is missing, the latter never occurs. This can be labeled as direct evidence of causality. When the elimination of confounding variables is not easy, or a direct observation of the dynamic processes is not possible, one is often forced to resort to statistical testing, which necessarily involves *ad hoc* thresholds, above which causal claims can be made. In this paper, we will present direct observations of causal links between plastic events in a soft glass, which has been shown to be a good proxy for earthquakes [4]. While the statistics of plastic and tectonic events are the same, we note however that this does not suggest a common underlying process.

Earthquakes cluster in the space-time-magnitude domain, which is most readily observed by sequences of aftershocks said to be triggered by a prior main event. The rate of occurrence of aftershocks follows the well-known Omori law [5]. The causal link implied between a mainshock and aftershock is assumed to be through static or dynamic triggering [6], but the direct observation of this link via relevant dynamic variables inside the Earth remains elusive. The techniques to identify aftershocks have included space-time window-based approaches [7–9], stochastic declustering of earthquakes modeled as a point process [10], evolving random graphs [11], machine learning techniques such as diffusion maps [12] and neural networks [13], and a nearest-neighbor (NN) rescaled space-time-magnitude metric [14,15]. This last method has seen wider adoption in seismology [4,16–20]. The NN metric combines the phenomenological Gutenberg-Richter (GR) law with the fact that earthquake epicenters have a fractal distribution and is an estimate of the number of expected events within a certain radius, time, and magnitude range [14]. The probability distribution of this NN measure is close to bimodal, with one mode corresponding to that of a Poissonian field and the other to clustered events. Our unambiguous causal catalog of aftershocks exhibits two triggering modes, each following Omori’s law with a distinct slope. Furthermore, by applying the NN measure to our catalog, we provide a validation to this widely used statistical declustering tool in seismology.

In this paper we first present a means of establishing causality by the direct observation of mainshocks and aftershocks, then we check whether aftershocks in our catalog follow Omori’s law, and finally whether the NN measure is indeed a valid tool to decluster parent-child catalogs. The aim of this paper is not to investigate the underlying mechanisms nor

Published by the American Physical Society under the terms of the [Creative Commons Attribution 4.0 International](https://creativecommons.org/licenses/by/4.0/) license. Further distribution of this work must maintain attribution to the author(s) and the published article’s title, journal citation, and DOI.

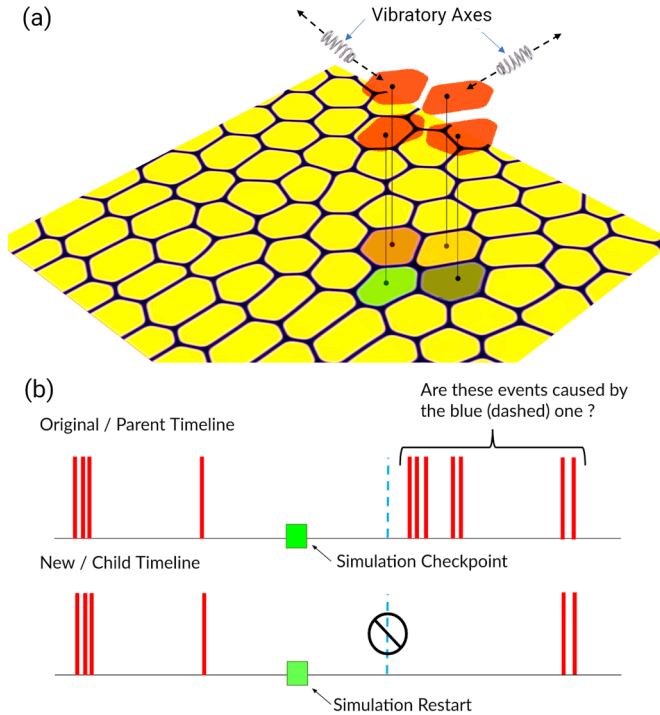


FIG. 1. (a) Density field of our binary fluid soft glass with drops of one component dispersed at a high packing fraction in the other. The geometrical shape of a quartet of neighboring drops about to undergo a topological rearrangement is extracted. Each drop is subjected to a vibratory forcing along an axis from the drop’s center to the quartet’s center of mass, thus turning the local potential energy hill into a valley and arresting the droplets. (b) Schematic approach for establishing causality. A simulation labeled the “parent” is run and events are identified. To find the causal aftershocks of a given event, a “child” simulation where this event is arrested is run starting from a checkpoint of the LB population just prior to said event. All subsequent events, which are present in the parent timeline but missing from the child timeline, are labeled aftershocks or, if otherwise, independent. Figure reproduced from the author’s own work [25].

the physical origins of the observations, but to report observations that confirm that NN allows one to separate mainshocks and aftershocks and that different triggering mechanisms very likely result in different Omori slopes.

## II. METHOD

To investigate event causality, we adopt a numerical scheme based on a multicomponent lattice Boltzmann (LB) method [21], which we have shown to be a good *in silico* earthquake proxy [4]. We briefly describe the method here. Our system comprises a binary fluid, with competing long- and short-range inter- and intrafluid interactions which promote frustration of the interface. At higher packing fractions, glassy dynamics sets in with very long relaxation times resulting in a soft glass [see Fig. 1(a)], aging behavior [21], and Herschel-Bulkley rheology [22]. The system relaxes through irreversible topological rearrangements of neighboring droplets which deform plastically. These plastic events, always comprising four droplets (a quartet) in two dimensions (2D), radiate a part of the released energy away from the site

and are accompanied by stress drops [23]. When experiencing a Couette shear slightly below the yield stress, the system exhibits a long-range correlation in stress and the plastic event sizes, duration, and interevent times follow well-established empirical seismic scaling laws [4,24].

Our method for establishing direct causality is sketched in Fig. 1(b). We first run our LB simulation with regular checkpoints of the LB populations and collect plastic event data, and this simulation run is labeled the “parent run.” For each event identified in the parent run, we rerun another LB simulation called the “child run” where the simulation is restarted from a checkpoint just prior to a target event, and where that event is stopped from occurring. We then check to see how the downstream dynamics differ in the child run—specifically which events from the parent run disappear and which remain the same.

In Ref. [25] we presented a method to stop a plastic event from occurring inspired by the stabilization of the Kapitza pendulum. Kapitza [26] showed that fast vibrations with a small amplitude could stabilize an inverted pendulum by separating the resulting vibrations into slow and fast components. Here, the term fast is relative to the natural frequency of the system which is slower. Kapitza then showed that the faster vibrations effectively modified the local potential landscape so that the vertical position became a point of stable equilibrium. In a similar vein, we applied small fast vibrations to the quartet of drops about to undergo a plastic event. This lowered the local potential energy hill, and since events only occur as a way to release energy, this prevented the event from occurring. This topological arrest of a quartet required modifications to the usual LB scheme as

$$f^* = (1 - \epsilon) \underbrace{\left( f - \frac{1}{\tau}(f - f^{\text{eq}}) + F \right)}_{\text{Normal LB update}} + \epsilon(f^{\text{eq}-\text{Arrest}}). \quad (1)$$

The normal LB update is highlighted, with  $f$  representing the LB population distribution,  $\tau$  being the time to relax to the local Maxwellian equilibrium  $f^{\text{eq}}$ , and  $F$  is the intra- and intermolecular forcing term. Just putting  $F$  to zero will not provide the desired clean catalog due to aging [21]. We modify this and introduce the term  $f^{\text{eq}-\text{Arrest}}$ , which corresponds to the equilibrium population distributions of the set of points making up the droplet quartet immediately prior to the event, and a scalar  $\epsilon$  which is a spatiotemporal function—spatially it takes the value of unity at the points belonging to the drop quartet and zero elsewhere while the temporal part is periodic with magnitude between 0 and 1. In effect what is achieved is an operation where the quartet is frozen in time and space, i.e., arrested and then released periodically. This can be visualized in Fig. 1(a) by imagining the four drops to be vibrating along an axis connecting their individual center of mass and the collective center of mass of the quartet. The amplitude of the vibrations is very small and is of the order of the random diffusive current in the interface, and we have demonstrated in Ref. [25] that this technique does not disturb neighboring drops and allows us to achieve a “clean” arrest of an event. Whenever we stop an event there is a stress redistribution, and given a sufficiently large amount of time, some new events will be created. We took care to ensure that for the duration

for which we have gathered statistics, no new events were present.

Using the modified LB scheme, we built a database of event sequences with the aim to analyze a large number of these sequences to extract causal relations. In this database, each event is associated to two simulations: a parent run where the event occurs and a child run where the event has been prevented from occurring. The criteria for classifying event pairs as being either causally connected or independent is as follows: Those events from the *parent* timeline which do not occur in the *child* timeline subsequent to a plastic event having been stopped, are said to be causally connected or in the language of seismology are aftershocks. On the other hand, those events from the *parent* timeline which reoccur at the exact same time and location in the *child* timeline despite the plastic event being stopped, are said to be independent events. The premise behind the above classification is simple. A change in the local topology due to a parent event manifests itself as a propagating disturbance and becomes the cause for triggering those events which have now disappeared after the parent has been stopped. In a similar vein, independent events have their origin in other factors but not the stopped event. All event pairs in our database are classified accordingly, yielding 1310 event-aftershock pairs. When a single event has multiple aftershocks we call it an aftershock sequence. Some sequences have several events and the causal chain can span a long time duration (up to 400k timesteps), while in other cases the chain terminates more quickly (30k timesteps).

### III. RESULTS

For every sequence or causal chain in our database, we calculated the time elapsed between the *parent* event and its *child* (aftershock) and this time difference is used to fit Omori's law. Omori's law, originating in seismology, as shown in Eq. (2), states that the rate  $r$  of aftershocks resulting from a parent earthquake scales roughly with the inverse of time. In practice, from earthquake catalogs it has been estimated that the exponent  $p \in [0.8, 1.5]$  with productivity  $k$  and time delay  $c$  being constant for a given system [5],

$$r = \frac{k}{(c + t)^p}, \quad (2)$$

where  $t$  is the time elapsed since the *parent* event. Given that we have access to the precise occurrence times of events and their aftershocks, evaluating the aftershock rate is straightforward. Inferring the three parameters in Omori's law, however, is an ill-posed optimization problem full of trade-offs. We opted for a Bayesian estimation [27], including a reparametrization, which separates the determination of the productivity  $k$  from the shape parameters  $p$  and  $c$ . Furthermore, in this reformulation, the shortest and longest elapsed times between parent and aftershock in the catalog determine a large part of the uncertainty in the shape parameters [27]. The advantage of the Bayesian analysis is that the formulation works directly with the occurrence times without having to construct  $r$ , which is not directly observed. It measures the degree of belief we have in Eq. (2) given some prior information. The prior we used is a noninformative Jeffreys prior on the reformulated productivity,  $p = 1$  and  $c = 1/c_{\max}$ ,

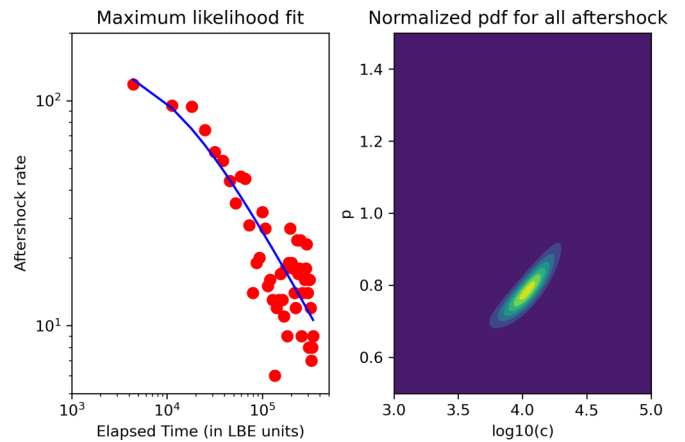


FIG. 2. Left panel: Aftershock rate against the time elapsed since the parent event. The observed rate (red circles) is derived from the histogram of our complete catalog of 1310 parent-aftershock pairs. The blue line corresponds to the curve from the Bayesian maximum likelihood parameters, which has been used to fit Eq. (2) and serves as an illustration only. Right panel: Normalized joint probability density for  $p$  and  $c$  from a Bayesian fit to Eq. (2) using the occurrence times of the same 1310 aftershocks in our database. The yellow contour has a value of 1 and the purple one a value of 0. The goodness of fit should be judged from the contours and the corresponding parameter uncertainties are given in the text.

where we searched for  $c \in [10^3, 10^5]$ . In Fig. 2, we plot the aftershock rate versus time elapsed since the *parent* event. Our Bayesian inference gives  $p = 0.78 \pm 0.03$ ,  $c = (10 \pm 3)10^3$ , and  $k = (232 \pm 51)10^3$ . There is a trade-off between  $p$  and  $c$ , but they do not depend on the maximum elapsed time used in the analysis. The uncertainties directly depend on the number of aftershocks and hence the maximum elapsed time in the catalog.  $k$  is independent of the shape parameters and increases linearly with the number of events in the catalog determined by the maximum elapsed time [27].

Since we know the position and timing of the aftershocks with respect to the main event, we can analyze the speed of information propagation  $v$  between the pairs. In this analysis, we only consider the first aftershock to each parent to avoid secondary effects due to triggering by other aftershocks and wave reflections from domain walls, which could bias estimates of information speed. In Fig. 3, we present the probability distribution of  $\log v$ . Also shown are two speeds,  $v_{\text{shear}}$  and  $v_{\text{sound}}$ , representative of our system. Our implementation gives us access to the bulk thermodynamic pressure and under the constraints of mass and momentum conservation and lattice isotropy, the speed of sound is then simply  $v_{\text{sound}} = \sqrt{dP/d\rho} = 1/\sqrt{3}$ . Since we are forcing our soft glass in a regime just below the yield stress, it has the properties of a solid, and thus can sustain both compression and shear waves, unlike fluids that cannot transmit shear waves.  $v_{\text{shear}} \approx 0.02$  has been determined previously for our system [28]. Roughly 80% of first aftershocks fall within the light cone of the elastic shear wave while all first aftershocks fall within the light cone of the speed of sound. The fact that almost 20% of events are triggered before the elastic shear waves can reach them is interesting. On closer inspection, we found that for those events, the involved droplets are either directly in contact with

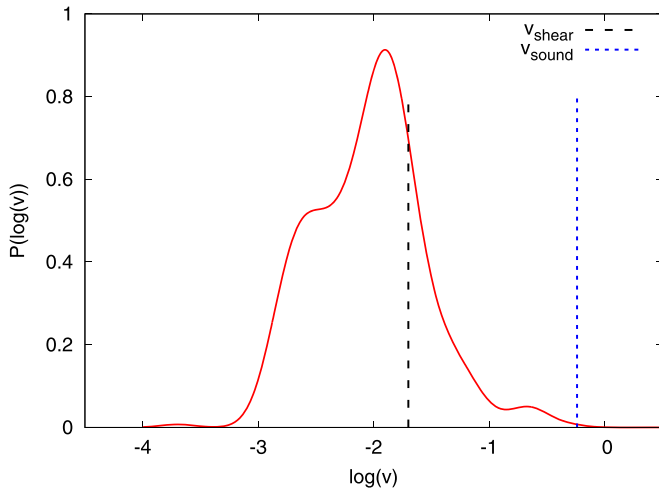


FIG. 3. Probability distribution of the log of speed ( $v$ ) of information propagation to the first aftershock. A kernel density estimate is applied to obtain the smooth distribution shown. The black dashed line indicates the speed of propagation of elastic shear waves ( $v_{\text{shear}} = 0.02$ ) and the blue dotted line shows the speed of sound ( $v_{\text{sound}} = 0.58$ ) in the lattice Boltzmann scheme.

the droplets belonging to the parent event or are second neighbors. Due to the constraints of geometry imposed by the rigid interface these neighbor drops are forced to deform almost simultaneously with the parent event compared to drops that are further away. In summary, all aftershocks in our system are triggered by two means: (i) by geometrical constraints (of a rigid interface) arising from the deformation of neighbors who are undergoing a plastic event and (ii) passing elastic shear wave perturbations that overcome the local balance of forces.

#### IV. DISCUSSION

We have identified two modes of event triggering, by contact and by passage of shear waves. This is similar to (quasi)static versus dynamic stress triggering identified in seismology [6,29]. Static stress triggering refers to the stress change just before an earthquake and after the dynamic stresses transported by seismic waves have dissipated, which then triggers an event on a nearby fault close to the Coulomb failure threshold. Quasistatic triggering takes viscous dissipation of static stresses into account. The oscillatory dynamic stresses transported by elastic waves have a longer reach, and especially surface waves can bring a region close to failure. We observe that events triggered by seismic waves can affect the whole medium and hence are spread out in time, while the contact events (static stress changes) act locally and fast (Fig. 3). Having clearly identified the two classes of triggered events, we fitted Omori's law to them both independently (Fig. 4). In our Bayesian analysis, it was shown [27] that the Omori parameters do not depend on the number (or begin and end times) of aftershock catalogs but the uncertainties do. The contact aftershocks occur quickly after the main event, and therefore we limited the shear wave triggered events to the same short time interval. This is to ensure that we can make a robust comparison between parameters. The interesting observation is that shear wave triggered events

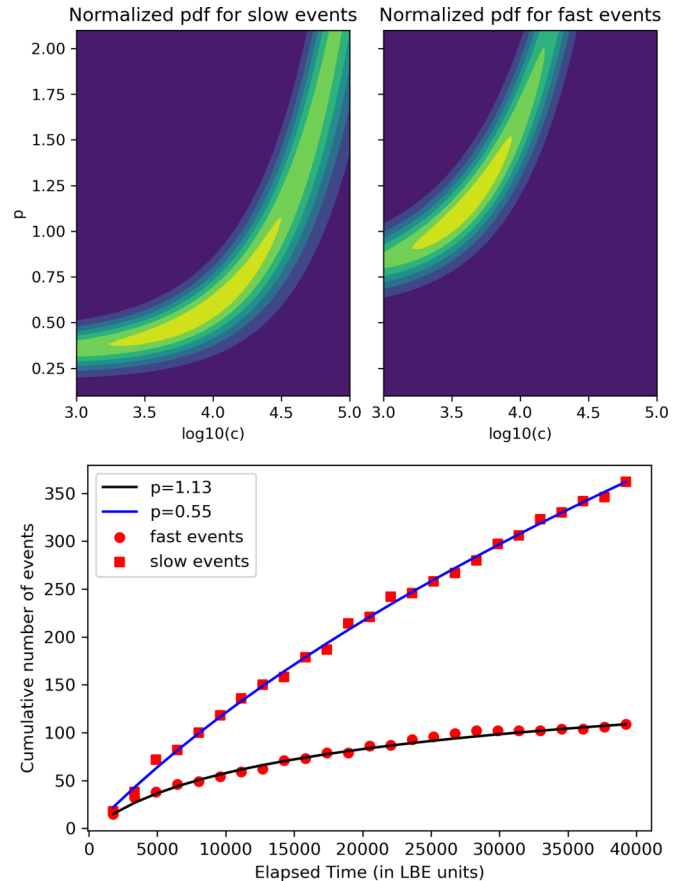


FIG. 4. Top: Normalized joined probability density for  $p$  and  $c$  [from Eq. (2)] for events triggered by contact (fast) mode (109 aftershocks) and shear wave (slow) mode (362 aftershocks). The yellow contour has a value of 1 and the purple one a value of 0. Bottom: Cumulative number of aftershocks which clearly shows that our most likely parameters fit the data very well. Additionally, the cumulative distributions are smooth without kinks, indicating that secondary aftershocks, which might be present, do not bias the analysis.

have a notably lower Omori slope  $p = 0.55 \pm 0.05$  (event rate decays more slowly) than contact events  $p = 1.13 \pm 0.10$ . Both series contain roughly the same order of events and therefore their uncertainties are comparable. We can thus state with 99% confidence (within 3 standard deviations) that the values of  $p$  do not overlap. The time delay  $c$  and the event productivity  $k$  are statistically not separable for the two modes. Given that a large range of Omori slopes has been reported in seismology, we suggest that it might be interesting to investigate whether static versus dynamic triggering also results in two distinct Omori slopes for earthquakes. In a spatial analysis of aftershocks [30], it appears that the density of aftershocks as a function of distance from the parent event also shows different power laws for static and dynamic triggering. Unfortunately our system is too small ( $1024 \times 1024$  LB units—roughly fitting 500 droplets) to derive spatial power laws. An additional question worth pursuing is whether the two observations in time (present paper) and space [30] might even be linked.

Aftershock identification in the case of earthquakes is more subjective and mostly statistical. Having a ground

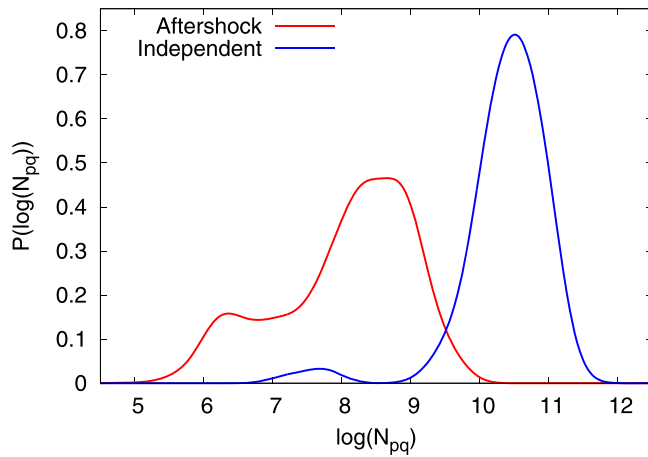


FIG. 5. Probability distribution of the nearest-neighbor “distance” measure  $N_{pq}$  of Eq. (3) with the red curve representing aftershocks and the blue curve representing independent events. The major peaks for the two scenarios show a clear bimodality of the combined distribution, as in the case of earthquakes. The highest peak of the aftershock distribution  $\log(N_{pq}) \approx 8.5$  corresponds to shear wave triggered events and the smaller peak  $\log(N_{pq}) \approx 6$  to contact aftershocks.

truth aftershock catalog puts us in a position to evaluate the popularly used statistical approach of the nearest-neighbor (NN) metric [15] in seismology. For every pair of events  $(i, j)$  in the event database, such that  $i$  occurred before  $j$ , the NN measure is defined as

$$N_{ij} = \Delta T (\Delta L)^{d_f} 10^{-B_{GR} \log M_i}, \quad (3)$$

where  $\Delta T = T_j - T_i$  is the interevent time,  $\Delta L$  is the spatial separation,  $d_f$  is the fractal dimension of event centers,  $B_{GR}$  is the slope of the Gutenberg-Richter law, and  $M_i$  is the magnitude of event  $i$ .  $\Delta T$  and  $\Delta L$  are directly available from our database of events,  $M_i$  is taken to be the squared displacement of the parent event, while  $B_{GR} = 0.7$  and  $d_f = 1.5$  are values from Ref. [4], as they used the same soft-glass model. Through empirical observations [17], it was shown that the distribution of  $N_{ij}$  for real earthquakes exhibits a bimodality, which permits discriminating between aftershocks and independent events. Since we already know which events

are aftershocks and which are independent, we plot the respective NN metric distribution in Fig. 5. The distributions of  $N_{ij}$  for aftershocks and independent events mainly show two distinct clusters. The aftershock cluster exhibits two peaks, a small one corresponding to the fast mode and a main one for the slow mode. The independent event cluster shows one dominant peak. There is some small overlap between aftershock and independent events where events are not perfectly separable. Thus we can state that the separation in distinct modes of the distribution of all event pairs is not a statistical artifact but emerges naturally from the combination of the distributions of aftershocks and independent events. Note that a synthetic earthquake catalog generated numerically from a Poisson point process would give a unimodal distribution.

## V. CONCLUSION

We devised a technique which allows us to separate plastic events into independent and triggered events or aftershocks. A Bayesian analysis showed that the aftershocks in our catalog follow Omori’s law. We further noticed that aftershocks are triggered by two different modes: by contact and by a passing shear wave. While the two classes of aftershocks independently follow Omori’s law, their temporal decay is significantly different. We suggest that this might allow seismologists to separate dynamically from statically triggered aftershocks, similar to aftershock density distributions as a function of distance. Finally, we showed that, in the absence of a direct way to establish causality, the popular nearest-neighbor metric used in seismology is indeed a good way to separate aftershocks from independent events.

## ACKNOWLEDGMENTS

This publication is part of the project Earthquake dynamics understanding their physics from modeling soft-glassy materials (with Project No. 680.93.14CSER022) of the research programme FOM – Industrial Partnership Programmes (IPP) FOM – Industrial Partnership Programmes (IPP) which is (partly) financed by the Dutch Research Council (NWO). The work is also (partly) sponsored by NWO domain Science for the use of supercomputer facilities.

- 
- [1] G. M. D’Ariano, Causality re-established, *Philos. Trans. R. Soc. A* **376**, 20170313 (2018).
  - [2] A. Summers, Common-sense causation in the law, *Oxford J. Legal Stud.* **38**, 793 (2018).
  - [3] S. Galea, M. Riddle, and G. A. Kaplan, Causal thinking and complex system approaches in epidemiology, *Int. J. Epidemiol.* **39**, 97 (2010).
  - [4] R. Benzi, P. Kumar, F. Toschi, and J. Trampert, Earthquake statistics and plastic events in soft-glassy materials, *Geophys. J. Int.* **207**, 1667 (2016).
  - [5] T. Utsu, Y. Ogata, and R. S. Matsu’ura, The centenary of the Omori formula for a decay law of aftershock activity, *J. Phys. Earth* **43**, 1 (1995).
  - [6] A. M. Freed, Earthquake triggering by static, dynamic and post seismic stress transfer, *Annu. Rev. Earth Planet. Sci.* **33**, 335 (2005).
  - [7] J. Gardner and L. Knopoff, Is the sequence of earthquakes in southern California, with aftershocks removed, Poissonian? *Bull. Seismol. Soc. Am.* **64**, 1363 (1974).
  - [8] M. D. Petersen, C. S. Mueller, M. P. Moschetti, S. M. Hoover, A. L. Llenos, W. L. Ellsworth, A. J. Michael, J. L. Rubinstein, A. F. McGarr, and K. S. Rukstales, 2016 one-year seismic hazard forecast for the Central and Eastern United States from induced and natural earthquakes, Open-File Report (2016), doi: 10.3133/ofr20161035.

- [9] L. Knopoff, Y. Y. Kagan, and R. Knopoff,  $b$  values for foreshocks and aftershocks in real and simulated earthquake sequences, *Bull. Seismol. Soc. Am.* **72**, 1663 (1982).
- [10] J. Zhuang, Y. Ogata, and D. Vere-Jones, Analyzing earthquake clustering features by using stochastic reconstruction, *J. Geophys. Res.* **109**, B05301 (2004).
- [11] S. Abe and N. Suzuki, Scale-free network of earthquakes, *Europhys. Lett.* **65**, 581 (2004).
- [12] Y. Bregman and N. Rabin, Aftershock identification using diffusion maps, *Seismol. Res. Lett.* **90**, 539 (2019).
- [13] Q. Zhang, T. Xu, H. Zhu, L. Zhang, H. Xiong, E. Chen, and Q. Liu, Aftershock detection with multi-scale description based neural network, in *Proceeding of the 2019 IEEE International Conference on Data Mining (ICDM)* (IEEE, New York, 2019), pp. 886–895.
- [14] M. Baiesi and M. Paczuski, Scale-free networks of earthquakes and aftershocks, *Phys. Rev. E* **69**, 066106 (2004).
- [15] I. Zaliapin, A. Gabrielov, V. Keilis-Borok, and H. Wong, Clustering Analysis of Seismicity and Aftershock Identification, *Phys. Rev. Lett.* **101**, 018501 (2008).
- [16] C. Gu, A. Y. Schumann, M. Baiesi, and J. Davidsen, Triggering cascades and statistical properties of aftershocks, *J. Geophys. Res. Solid Earth* **118**, 4278 (2013).
- [17] I. Zaliapin and Y. Ben-Zion, Earthquake clusters in southern California I: Identification and stability, *J. Geophys. Res.: Solid Earth* **118**, 2847 (2013).
- [18] Q. Zhang and P. M. Shearer, A new method to identify earthquake swarms applied to seismicity near the San Jacinto Fault, California, *Geophys. J. Int.* **205**, 995 (2016).
- [19] J. Moradpour, S. Hainzl, and J. Davidsen, Nontrivial decay of aftershock density with distance in southern California, *J. Geophys. Res.: Solid Earth* **119**, 5518 (2014).
- [20] I. Zaliapin and Y. Ben-Zion, Earthquake decluttering using the nearest-neighbor approach in space-time-magnitude domain, *J. Geophys. Res.: Solid Earth* **125**, e2018B017120 (2020).
- [21] R. Benzi, M. Sbragaglia, S. Succi, M. Bernaschi, and S. Chibbaro, Mesoscopic lattice Boltzmann modeling of soft-glass systems: Theory and simulations, *J. Chem. Phys.* **131**, 104903 (2009).
- [22] R. Benzi, M. Bernaschi, M. Sbragaglia, and S. Succi, Herschel-Bulkley rheology from lattice kinetic theory of soft glassy materials, *Europhys. Lett.* **91**, 14003 (2010).
- [23] R. Benzi, M. Sbragaglia, P. Perlekar, M. Bernaschi, S. Succi, and F. Toschi, Direct evidence of plastic events and dynamic heterogeneities in soft-glasses, *Soft Matter* **10**, 4615 (2014).
- [24] P. Kumar, E. Korkolis, R. Benzi, D. Denisov, A. Niemeijer, P. Schall, F. Toschi, and J. Trampert, On interevent time distributions of avalanche dynamics, *Sci. Rep.* **10**, 626 (2020).
- [25] P. Kumar, R. Benzi, J. Trampert, and F. Toschi, A multi-component lattice Boltzmann approach to study the causality of plastic events, *Philos. Trans. R. Soc. A* **378**, 20190403 (2020).
- [26] P. L. Kapitza, Dynamical stability of a pendulum when its point of suspension vibrates, and pendulum with a vibrating suspension, in *Collected Papers of P. L. Kapitza*, edited by D. ter Haar (Pergamon, New York, 1965), Vol. 2, p. 714.
- [27] M. Holschneider, C. Narteau, P. Shebalin, Z. Peng, and D. Schorlemmer, Bayesian analysis of the modified Omori law, *J. Geophys. Res.: Solid Earth* **117**, B06317 (2012).
- [28] R. Benzi, M. Bernaschi, M. Sbragaglia, and S. Succi, Rheological properties of soft glassy flows from hydro-kinetic simulations, *Europhys. Lett.* **104**, 48006 (2013).
- [29] D. Hill and S. Prejean, Dynamic triggering, in *Treatise on Geophysics*, edited by G. Schubert, 2nd ed. (Elsevier, Oxford, 2015), pp. 273–304.
- [30] K. Felzer and E. E. Brodsky, Decay of aftershock density with distance indicates triggering by dynamic stress, *Nature (London)* **441**, 735 (2006).